Металлофиз. новейшие технол. / Metallofiz. Noveishie Tekhnol.
2017, т. 39, № 5, сс. 567–578 / DOI: 10.15407/mfint.39.05.0567
Оттиски доступны непосредственно от издателя
Фотокопирование разрешено только
в соответствии с лицензией

ФАЗОВЫЕ ПРЕВРАЩЕНИЯ

PACS numbers: 61.50.Ks, 62.20.fg, 77.80.B-, 81.30.Kf, 83.10.Tv

Modes and Twinning Stresses of Martensite Variants Rearrangements in Near-Stoichiometric Ni_2MnGa Single Crystal

V. Soolshenko and V. Beloshapka*

G. V. Kurdyumov Institute for Metal Physics, N.A.S. of Ukraine,
36 Academician Vernadsky Blvd.,
UA-03142 Kyiv, Ukraine
**Berdyansk State Pedagogical University,*
4 Schmidt Str.,
UA-36244 Berdyansk, Ukraine

The sequences of the thermally induced martensitic and intermartensitic $L2_1 \rightarrow 10M \rightarrow 14M \rightarrow L1_0$ and $L1_0 \rightarrow 14M \rightarrow 10M \rightarrow L2_1$ transformations are observed in $Ni_{50.6}Mn_{28.5}Ga_{20.9}$ single crystal on the cooling and heating branches of a thermal cycle. The modes of stress-induced intervariant transitions in the $10M$, $14M$, and $L1_0$ martensites are investigated on the basis of matrix approach, and the stresses of orientation-variants' rearrangements are determined as a function of martensite structure, transition mode, and temperature. The twinning stress decreases along the $L1_0$, $14M$, and $10M$ martensites with a decrease of period of a nanotwinned structure.

Key words: shape-memory alloys, Ni_2MnGa, martensitic transformation, orientation variant, intervariant transition, twinning stress.

Послідовності термічно індукованих мартенситних і міжмартенситних перетворень $L2_1 \rightarrow 10M \rightarrow 14M \rightarrow L1_0$ і $L1_0 \rightarrow 14M \rightarrow 10M \rightarrow L2_1$ спостерігаються у $Ni_{50,6}Mn_{28,5}Ga_{20,9}$-монокристалі у термічному циклі охолодження та нагрівання. Досліджено види індукованих напругою міжваріантних переходів у $10M$-, $14M$- і $L1_0$-мартенситах на основі матричного опису та визначено напруги перерозподілу орієнтаційних варіянтів, залежно від структури мартенситу, виду переходу та температури. Напруга двійникування зменшується уздовж $L1_0$-, $14M$-, $10M$-мартенситів із зменшенням

Corresponding author: Valeriy Konstantinovich Soolshenko
E-mail: soolsh@imp.kiev.ua

Please cite this article as: V. Soolshenko and V. Beloshapka, Modes and Twinning Stresses of Martensite Variants Rearrangements in Near-Stoichiometric Ni_2MnGa Single Crystal, *Metallofiz. Noveishie Tekhnol.*, **39**, No. 5: 567–578 (2017), DOI: 10.15407/mfint.39.05.0567.

періоду нанодвійникованої структури.

Ключові слова: стопи з пам'яттю форми, Ni_2MnGa, мартенситне перетворення, орієнтаційний варіянт, міжваріянтний перехід, напруга двійникування.

Последовательности термически индуцированных мартенситных и межмартенситных превращений $L2_1 \rightarrow 10M \rightarrow 14M \rightarrow L1_0$ и $L1_0 \rightarrow 14M \rightarrow 10M \rightarrow L2_1$ наблюдаются в $Ni_{50,6}Mn_{28,5}Ga_{20,9}$-монокристалле в термическом цикле охлаждения и нагрева. Исследованы виды индуцированных напряжением межвариантных переходов в $10M$-, $14M$- и $L1_0$-мартенситах на основе матричного описания и определены напряжения перераспределения ориентационных вариантов в зависимости от структуры мартенсита, вида перехода и температуры. Напряжение двойникования уменьшается вдоль $L1_0$-, $14M$-, $10M$-мартенситов с уменьшением периода нанодвойникованной структуры.

Ключевые слова: сплавы с памятью формы, Ni_2MnGa, мартенситное превращение, ориентационный вариант, межвариантный переход, напряжение двойникования.

(Received April 18, 2017)

1. INTRODUCTION

The martensitic transformations in ferromagnetic Ni–Mn–Ga alloys attract much attention for many years, since they are associated with the large magnetic field induced strain (MFIS). Reversible magnetic field induced strains up to 12% were reported for the alloys with compositions near Ni_2MnGa compound [1–4].

The near-stoichiometric Ni_2MnGa Heusler alloys with b.c.c. ($L2_1$ ordered) austenite structure undergo transformation to one of several martensites. The f.c.t. ($L1_0$ ordered) tetragonal martensite is thought to be the ground state of martensitic phase. The nanotwinned $10M$ tetragonal and $14M$ orthorhombic martensites are resulted from stacking of nearly close-packed {111} basal planes, which originate from $\{110\}_{\text{b.c.c.}}$ planes of austenite, with the $(3\bar{2})_2$ and $(5\bar{2})_2$ sequences, correspondingly [5–14].

Martensitic transformation lowers the crystalline point symmetry of parent cubic phase. It is followed by two events: (1) the transformation strain accommodates by formation of multiple martensitic orientational variants and (2) the easy magnetization axis and easy magnetization plane appear in the tetragonal $10M$ ($c/a < 1$) and $L1_0$ ($c/a > 1$) martensitic variants, respectively. At magnetic field applied, the variants have different free energy dependent on direction of easy magnetization.

The MFIS phenomenon is caused by grows of volume fraction of

preferentially oriented variant controlled by motion of intervariant twin boundaries. The rearrangement of martensitic variants results in shape strain that is as large as the tetragonality of crystalline lattice.

The MFIS is possible if the magnetocrystalline anisotropy energy of martensitic variant is high enough to move the intervariant interfaces [15]. Thus, an achievement of low twinning stress is one of the aims in design of MFIS alloys.

In the paper below, we report the modes and twinning stresses of stress-induced intervariant transitions in the $10M$, $14M$ and $L1_0$ martensites of near-stoichiometric Ni_2MnGa single crystal.

2. EXPERIMENTAL PROCEDURES

The $Ni_{50.6}Mn_{28.5}Ga_{20.9}$ alloy was prepared by melting in an induction furnace in argon atmosphere, followed by casting into alumina crucible. The single crystal was grown with using the Bridgeman method and annealed for the homogenization at 1273 K for 72 hours. The rectangular prismatic sample with dimensions of edges $5\times6\times7$ mm^3 was cut from a single crystal with a low speed diamond saw and electropolished in 30% nitric acid–methanol solution. The edges of the sample were parallel to the $[100]_c$, $[010]_c$ and $[001]_c$ directions of the cubic lattice of austenite phase.

The low field magnetic susceptibility and x-ray diffraction measurements were used to determine the temperatures of martensitic transformations, martensite crystal structures and lattice parameters. The variant structure of martensites was distinguished with two-surface metallographic analysis. Initial single-variant state of martensite sample was achieved by mechanical training.

Compression mechanical tests were carried out at 10^{-3} s^{-1} strain rate. The whole investigation has been fulfilled with the same single-crystalline sample.

3. RESULTS AND DISCUSSION

3.1. Thermally Induced Structural Transitions

The ferromagnetic transition at Curie temperature 370 K and four successive structural transitions were observed on cooling of $Ni_{50.6}Mn_{28.5}Ga_{20.9}$ sample (Fig. 1).

The first transition at temperature 332 K was martensitic transformation of austenitic $L2_1$ ordered cubic phase (A) with lattice parameter 0.5839 nm in nanotwinned $10M$ tetragonal martensite. Lattice parameters of the martensite are equal to $a = b = 0.594$ nm, $c = 0.557$ nm (in cubic crystal-lattice basis $\mathbf{x}_i$ of austenite phase).

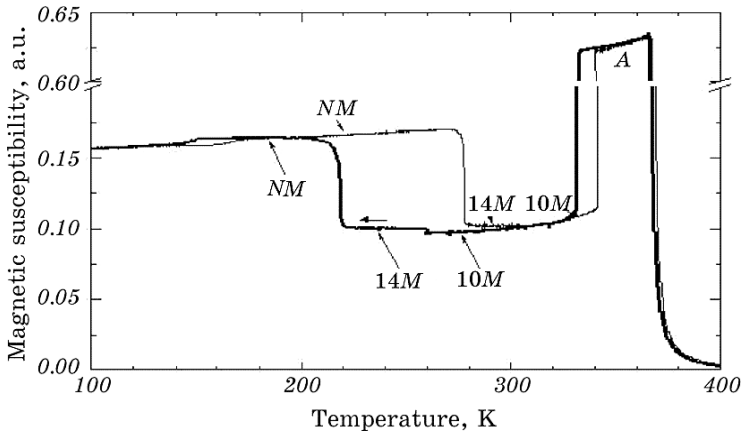

Fig. 1. Temperature dependence of magnetic susceptibility.

As temperature being decreased, two successive intermartensitic transformations occurred. At temperature 259 K, the 10*M* tetragonal martensite was transformed into the nanotwinned 14*M* orthorhombic martensite. The lattice parameters of 14*M* martensite are equal to $a = 0.616$ nm, $b = 0.580$ nm, $c = 0.553$ nm.

At temperature 215 K, the 14*M* orthorhombic martensite transformed into nontwinned tetragonal martensite (*NM*) with lattice parameters equal $a = b = 0.548$ nm, $c = 0.655$ nm. The structure of *NM* martensite can be described by tetragonal $L1_0$ ordered unit cell doubled because of $L2_1$ ordering of austenite phase.

The transition to nonidentified structure (*X*) was observed at temperature 149 K. The temperatures of reverse phase transformations during heating are as follows: $T^{X \to NM} = 169$ K, $T^{NM \to 14M} = 277$ K, $T^{14M \to 10M} = 307$ K, $T^{10M \to A} = 341$ K.

3.2. Modes of Stress-Induced Intervariant Transitions

Before mechanical tests on intervariant transitions, the variant struc-

TABLE 1. Lattice parameters of austenite (*A*) and martensitic (10*M*, 14*M* and *NM*) phases at temperatures 340 K (*A*), 297 K (10*M*, 14*M*) and 210 K (*NM*).

Axes	Lattice parameters, nm			
	A ($L2_1$)	10*M*	14*M*	*NM* ($L1_0$)
x_1	0.5839	0.594	0.616	0.655
x_2	0.5839	0.594	0.580	0.548
x_3	0.5839	0.557	0.553	0.548

ture of martensites has to be described. We propose matrix description of variant structures and intervariant transitions that would be especially suitable for the unorthogonal crystalline bases (Table 1).

The cubic-to-tetragonal $L2_1 \rightarrow 10M$ martensitic transformation reduces the point symmetry of a crystal lattice, and three different orientational variants with tetragonal axis parallel to one of $<100>_c$ directions of austenite cubic phase can be generated. These variants can be designated by three transformation strain matrices:

$$\varepsilon_{ij}^{10M}(1) = \begin{pmatrix} \varepsilon_{11}^{10M} & 0 & 0 \\ 0 & \varepsilon_{11}^{10M} & 0 \\ 0 & 0 & \varepsilon_{33}^{10M} \end{pmatrix}, \quad \varepsilon_{ij}^{10M}(2) = \begin{pmatrix} \varepsilon_{11}^{10M} & 0 & 0 \\ 0 & \varepsilon_{33}^{10M} & 0 \\ 0 & 0 & \varepsilon_{11}^{10M} \end{pmatrix},$$

$$\varepsilon_{ij}^{10M}(3) = \begin{pmatrix} \varepsilon_{33}^{10M} & 0 & 0 \\ 0 & \varepsilon_{11}^{10M} & 0 \\ 0 & 0 & \varepsilon_{11}^{10M} \end{pmatrix}, \qquad (1)$$

where $\varepsilon_{11}^{10M} = (a_t^{10M} - a_c^A) / a_c^A = 0.017$, $\varepsilon_{33}^{10M} = (c_t^{10M} - a_c^A / a_c^A) = -0.046$ and $a_c^A = 0.5839$ nm, $a_t^{10M} = 0.594$ nm, $c_t^{10M} = 0.557$ nm are the crystal lattice parameters of austenite cubic and $10M$ martensite tetragonal phases.

At the intermartensitic $10M \rightarrow 14M$ transformation, the orthorhombic $14M$ martensite is a final phase. Six orientational variants of $14M$ martensite are defined by following strain matrices:

$$\varepsilon_{ij}^{14M}(1) = \begin{pmatrix} \varepsilon_{11}^{14M} & 0 & 0 \\ 0 & \varepsilon_{22}^{14M} & 0 \\ 0 & 0 & \varepsilon_{33}^{14M} \end{pmatrix}, \quad \varepsilon_{ij}^{14M}(2) = \begin{pmatrix} \varepsilon_{11}^{14M} & 0 & 0 \\ 0 & \varepsilon_{33}^{14M} & 0 \\ 0 & 0 & \varepsilon_{22}^{14M} \end{pmatrix},$$

$$\varepsilon_{ij}^{14M}(3) = \begin{pmatrix} \varepsilon_{22}^{14M} & 0 & 0 \\ 0 & \varepsilon_{33}^{14M} & 0 \\ 0 & 0 & \varepsilon_{11}^{14M} \end{pmatrix}, \quad \varepsilon_{ij}^{14M}(4) = \begin{pmatrix} \varepsilon_{22}^{14M} & 0 & 0 \\ 0 & \varepsilon_{11}^{14M} & 0 \\ 0 & 0 & \varepsilon_{33}^{14M} \end{pmatrix}, \qquad (2)$$

$$\varepsilon_{ij}^{14M}(5) = \begin{pmatrix} \varepsilon_{33}^{14M} & 0 & 0 \\ 0 & \varepsilon_{11}^{14M} & 0 \\ 0 & 0 & \varepsilon_{22}^{14M} \end{pmatrix}, \quad \varepsilon_{ij}^{14M}(6) = \begin{pmatrix} \varepsilon_{33}^{14M} & 0 & 0 \\ 0 & \varepsilon_{22}^{14M} & 0 \\ 0 & 0 & \varepsilon_{11}^{14M} \end{pmatrix},$$

where $\varepsilon_{11}^{14M} = (a_o^{14M} - a_c^A) / a_c^A = 0.055$, $\varepsilon_{22}^{14M} = (b_o^{14M} - a_c^A) / a_c^A = -0.007$, $\varepsilon_{33}^{14M} = (c_o^{14M} - a_c^A) / a_c^A = -0.053$ and $a_c^A = 0.5839$, $a_o^{14M} = 0.616$, $b_o^{14M} = 0.580$, $c_o^{14M} = 0.553$ nm are the crystal lattice parameters of the aus-

tenite cubic and $14M$ martensite orthorhombic phases.

Finally, three variants of tetragonal NM martensite are defined by strain matrices:

$$\varepsilon_{ij}^{NM}(1) = \begin{pmatrix} \varepsilon_{11}^{NM} & 0 & 0 \\ 0 & \varepsilon_{22}^{NM} & 0 \\ 0 & 0 & \varepsilon_{22}^{NM} \end{pmatrix}, \quad \varepsilon_{ij}^{NM}(2) = \begin{pmatrix} \varepsilon_{22}^{NM} & 0 & 0 \\ 0 & \varepsilon_{11}^{NM} & 0 \\ 0 & 0 & \varepsilon_{22}^{NM} \end{pmatrix},$$

$$\varepsilon_{ij}^{NM}(3) = \begin{pmatrix} \varepsilon_{22}^{NM} & 0 & 0 \\ 0 & \varepsilon_{22}^{NM} & 0 \\ 0 & 0 & \varepsilon_{11}^{NM} \end{pmatrix}, \tag{3}$$

where $\varepsilon_{11}^{NM} = \dfrac{c_t^{NM} - a_c^A}{a_c^A} = 0.122$, $\varepsilon_{22}^{NM} = \dfrac{a_t^{NM} - a_c^A}{a_c^A} = -0.061$ and $a_c^A = 0.5839$ nm, $a_t^{NM} = 0.548$ nm, $c_t^{NM} = 0.655$ nm are the crystal lattice parameters of austenite cubic and NM martensite tetragonal phases.

The variant rearrangements in the $10M$, $14M$ and NM martensites were examined in two-stage orthogonal loading experiments. The additional $\mathbf{e}_i$ basis formed by edges of the sample in initial austenitic state was used to determine the loading direction, sample shape, and orientation.

Under loading, the variant structure of martensite crystal is determined by tendency to minimize the total free energy of the crystal and loading device,

$$\min_{\alpha \in \{10M, 14M, NM\}} \int_V \left[\text{const} - \sigma_{ij} \varepsilon_{ij}^{\alpha}(k) \right] dV . \tag{4}$$

Therefore, the appropriate loading can stimulate a variant rearrangement.

Mechanical tests of $10M$ martensite were carried out at temperatures of $10M$ martensite phase stability on cooling and heating branches of thermal cycle (Figs. 1 and 3). At the first stage of mechanical testing, the sample of $10M$ martensite in single-variant state defined by $\varepsilon_{ij}^{10M}(1)$ strain matrix (that is the $10M$ variant 1 with short tetragonal axis $\mathbf{c}_t$ oriented along $\mathbf{e}_3$) was loaded in compression along $\mathbf{e}_2$ sample edge by stress $\sigma_2 = (0, -\sigma, 0)$. For this loading, the $10M$ variant 1 became unstable and rearrangement ($\varepsilon_{ij}^{10M}(1) \rightarrow \varepsilon_{ij}^{10M}(2)$) occurred (Fig. 2, $10Mac$).

At this rearrangement started from $10M$ variant 1 and finished with $10M$ variant 2, the transient microstructures were observed that were composed of these two variants in (011) twin-related conjunction. The increase of volume fraction of $10M$ variant 2 was controlled by

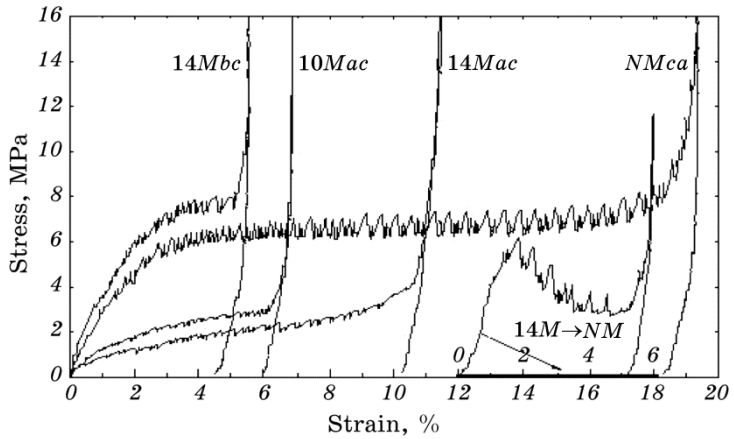

Fig. 2. Stress–strain curves for the intervariant transitions in the $10M$, $14M$, NM martensites and the intermartensitic $14M \rightarrow NM$ transformation.

(011) twin boundary motion. Because of $(\varepsilon_{ij}^{10M}(1) \rightarrow \varepsilon_{ij}^{10M}(2))$ transition, the short tetragonal $\mathbf{c}_t$ axis of $10M$ martensite was $\pi/2$ turned around $\mathbf{e}_1$ axis of the sample and consequently crystalline $\mathbf{a}_t$ axis was replaced by $\mathbf{c}_t$ axis along $\mathbf{e}_2$ sample edge ($10Mac$ mode of intervariant transition).

At the second stage of loading cycle being auxiliary, the sample was $\pi/2$ turned in grips of testing machine and the $10M$ variant 2 was loaded with $\sigma_3 = (0,0,-\sigma)$. The intervariant $(\varepsilon_{ij}^{10M}(2) \rightarrow \varepsilon_{ij}^{10M}(1))$ transition restored the initial variant structure and shape of the sample. The evolution of sample shape strain during loading cycle has some features.

The strain step across the twin boundary between the first and second orientational variants,

$$\Delta\varepsilon_{ij}^{10M}(12) = \varepsilon_{ij}^{10M}(2) - \varepsilon_{ij}^{10M}(1) =$$

$$= \varepsilon_{11}^{10M} - \varepsilon_{33}^{10M} \begin{pmatrix} 0 & 0 & 0 \\ 0 & \bar{1} & 0 \\ 0 & 0 & 1 \end{pmatrix} = 0.063 \begin{pmatrix} 0 & 0 & 0 \\ 0 & \bar{1} & 0 \\ 0 & 0 & 1 \end{pmatrix}, \tag{5}$$

is a plane strain. Therefore, the size of the sample edge along $\mathbf{e}_1$ is invariable in the loading cycle. The calculated strains along $\mathbf{e}_2$ and $\mathbf{e}_3$ axes are equal to 0.063 at the complete $10Mac$ intervariant transition. These strains are in agreement with experimentally measured ones (Fig. 2, $10Mac$).

This mode of intervariant transition in $10M$ martensite can be denoted as $10Mac$ because the transition interchanges the **a** and **c** crystal axes in $\mathbf{e}_i$ basis by the $\pi/2$ rotation around the third axis.

An essential feature of mechanical properties of $14M$ martensite is

existence of three modes of intervariant transitions. In the stress-free $14M$ martensite, which was assumed orthorhombic, six orientational variants (2) have an equal free energy. Under loading, three modes of intervariant transitions are possible. If to begin with orientational $\varepsilon_{ij}^{14M}(1)$ variant, the intervariant transitions can be realized by plane strain processes that are distinguished by following shape strains:

$$\Delta\varepsilon_{ij}^{14M}(12) = \varepsilon_{ij}^{14M}(2) - \varepsilon_{ij}^{14M}(1) =$$

$$= \varepsilon_{22}^{14M} - \varepsilon_{33}^{14M} \begin{pmatrix} 0 & 0 & 0 \\ 0 & \bar{1} & 0 \\ 0 & 0 & 1 \end{pmatrix} = 0.046 \begin{pmatrix} 0 & 0 & 0 \\ 0 & \bar{1} & 0 \\ 0 & 0 & 1 \end{pmatrix}, \tag{6}$$

$$\Delta\varepsilon_{ij}^{14M}(14) = \varepsilon_{ij}^{14M}(4) - \varepsilon_{ij}^{14M}(1) =$$

$$= \varepsilon_{11}^{14M} - \varepsilon_{22}^{14M} \begin{pmatrix} \bar{1} & 0 & 0 \\ 0 & 1 & 0 \\ 0 & 0 & 0 \end{pmatrix} = 0.062 \begin{pmatrix} \bar{1} & 0 & 0 \\ 0 & 1 & 0 \\ 0 & 0 & 0 \end{pmatrix}, \tag{7}$$

$$\Delta\varepsilon_{ij}^{14M}(16) = \varepsilon_{ij}^{14M}(6) - \varepsilon_{ij}^{14M}(1) =$$

$$= \varepsilon_{11}^{14M} - \varepsilon_{33}^{14M} \begin{pmatrix} \bar{1} & 0 & 0 \\ 0 & 0 & 0 \\ 0 & 0 & 1 \end{pmatrix} = 0.108 \begin{pmatrix} \bar{1} & 0 & 0 \\ 0 & 0 & 0 \\ 0 & 0 & 1 \end{pmatrix}. \tag{8}$$

These intervariant transitions belong to the $14Mbc$ (6), $14Mab$ (7) and $14Mac$ (8) transition modes (Fig. 3).

Under cooling below 259 K, the intermartensitic $10M \rightarrow 14M$ transformation occurred. The sample of $14M$ martensite in $\varepsilon_{ij}^{14M}(1)$ single-variant state was sequentially loaded in $\mathbf{e}_2\mathbf{e}_3$ plane with stresses

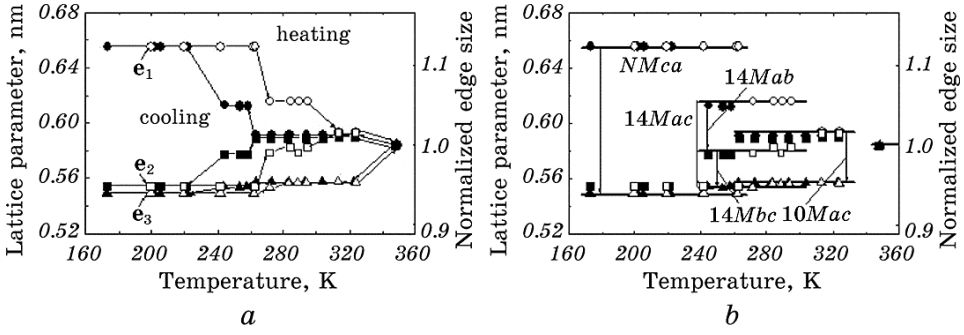

Fig. 3. Temperature dependences of sample edge sizes ($\mathbf{e}_1$, $\mathbf{e}_2$, $\mathbf{e}_3$) on the cooling and heating branches of thermal cycle (*a*) and scheme of intervariant transition modes (*b*).

$\sigma_2 = (0,-\sigma,0)$ and $\sigma_3 = (0,0,-\sigma)$, which induced two successive intervariant transitions, $(\varepsilon_{ij}^{14M}(1) \to \varepsilon_{ij}^{14M}(2))$ and $(\varepsilon_{ij}^{14M}(2) \to \varepsilon_{ij}^{14M}(1))$, controlled by (011) twin boundary motion. These intervariant transitions are related to $14Mbc$ mode (Fig. 2, $14Mbc$ and Fig. 3, *b*).

Under subsequent cooling below 215 K, the intermartensitic $14M \to NM$ transformation occurred. Because loading of NM martensite variant $\varepsilon_{ij}^{NM}(1)$ in $\mathbf{e}_2\mathbf{e}_3$ plane could induce only degenerated transition of the $NMaa$ mode, the loads with $\sigma_1 = (-\sigma,0,0)$ and $\sigma_3 = (0,0,-\sigma)$ in $\mathbf{e}_1\mathbf{e}_3$ plane were used, and the $NMca$ intervariant transitions, $(\varepsilon_{ij}^{NM}(1) \to \varepsilon_{ij}^{NM}(3))$ and $(\varepsilon_{ij}^{NM}(3) \to \varepsilon_{ij}^{NM}(1))$, controlled by (101) twin boundary motion were observed (Fig. 2, $NMca$ and Fig. 3). The shape strains of $(\varepsilon_{ij}^{NM}(1) \to \varepsilon_{ij}^{NM}(3))$ transition are given by

$$\Delta\varepsilon_{ij}^{NM}(13) = \varepsilon_{ij}^{NM}(3) - \varepsilon_{ij}^{NM}(1) = \\ = \varepsilon_{22}^{NM} - \varepsilon_{11}^{NM} \begin{pmatrix} \bar{1} & 0 & 0 \\ 0 & 0 & 0 \\ 0 & 0 & 1 \end{pmatrix} = 0.183 \begin{pmatrix} \bar{1} & 0 & 0 \\ 0 & 0 & 0 \\ 0 & 0 & 1 \end{pmatrix} \quad (9)$$

and coincide with experimentally measured $NMca$ strain (Fig. 2).

For the single variant state of the crystal, the sizes of crystal edges measured in $\mathbf{e}_i$ basis are proportional to corresponding lattice parameters measured in cubic $\mathbf{x}_i$ basis of austenite phase. For this reason, the scale of crystal lattice parameter was plotted at the left side of Fig. 3, *a*. The lattice parameters of austenite phase and the $10M$, $14M$, NM martensites are designated by solid lines on Fig. 3, *b*. It can be seen that the lattice parameters estimated for the martensites from crystal size measurements are well close to the parameters measured with x-ray diffraction method. This coincidence validates completeness of intervariant transitions and its modes.

On the heating branch of a thermal cycle, the intermartensitic $NM \to 14M$ transformation occurred at 277 K. The $14M$ martensite variant $\varepsilon_{ij}^{14M}(1)$ was two-stage loaded in $\mathbf{e}_1\mathbf{e}_3$ plane by stresses $\sigma_1 = (-\sigma,0,0)$ and $\sigma_3 = (0,0,-\sigma)$, which induced successive intervariant $(\varepsilon_{ij}^{14M}(1) \to \varepsilon_{ij}^{14M}(6))$ and $(\varepsilon_{ij}^{14M}(6) \to \varepsilon_{ij}^{14M}(1))$ transitions controlled by (101) twin boundary motion. These intervariant transitions belong to $14Mac$ mode (Fig. 2 and Fig. 3).

At subsequent heating above 307 K, the intermartensitic $14M \to 10M$ transformation occurred. Two-stage mechanical testing of $10M$ martensite variant $\varepsilon_{ij}^{10M}(1)$ with loads $\sigma_3 = (0,0,-\sigma)$ and $\sigma_1 = (-\sigma,0,0)$ induced the $10Mac$ intervariant $(\varepsilon_{ij}^{10M}(1) \to \varepsilon_{ij}^{10M}(3))$ and $(\varepsilon_{ij}^{10M}(3) \to \varepsilon_{ij}^{10M}(1))$ transitions controlled by (101) twin boundary motion. These intervariant transitions are identical to $10Mac$ transitions on the cooling branch of a thermal cycle (Fig. 3). The modes of intervariant transitions are summarized in Table 2.

It is worth to note that the nanotwinned $10M$ and $14M$ martensites, which discussed to be transient adaptive phases [16, 11, 17–18], were surprisingly stable to mechanical disturbance. The stresses caused intervariant transitions in nanotwinned martensites were insufficient to initiate the intermartensitic transformation of $10M$ and $14M$ martensites to perfect NM martensite. The only exception was the intermartensitic $14M \rightarrow NM$ transformation occurred at temperature 220 K that is 5 K above the temperature $T^{14M \rightarrow NM} = 215$ K of stress-free intermartensitic $14M \rightarrow NM$ transformation. The stress–strain diagram of intermartensitic $(\varepsilon_{ij}^{14M}(1) \rightarrow \varepsilon_{ij}^{NM}(1))$ transformation induced by stress $\sigma_2 = (0, -\sigma, 0)$ are shown at Fig. 2. The experimentally measured shape strains of $14M \rightarrow NM$ transformation are in accordance with calculated ones:

$$\Delta\varepsilon^{14M \rightarrow NM}(11) = \varepsilon_{ij}^{NM}(1) - \varepsilon_{ij}^{14M}(1) =$$

$$= \begin{pmatrix} \varepsilon_{11}^{NM} - \varepsilon_{11}^{14M} & 0 & 0 \\ 0 & \varepsilon_{33}^{NM} - \varepsilon_{22}^{14M} & 0 \\ 0 & 0 & \varepsilon_{33}^{NM} - \varepsilon\varepsilon_{33}^{14M} \end{pmatrix} = \tag{10}$$

$$= \begin{pmatrix} 0.067 & 0 & 0 \\ 0 & -0.054 & 0 \\ 0 & 0 & -0.008 \end{pmatrix}.$$

3.3. Stresses of Intervariant Transitions

Stresses of variant rearrangements were measured at a half of intervariant transition strains. The stresses are dependent on martensite structure, mode of intervariant transition and temperature (Fig. 4, *a*).

To compare the mobility of twin boundary in various martensites, it is useful to normalize the measured stresses. The stress-induced rearrangement of martensite variants can be considered as a transition of unstable loaded thermodynamic system crystal + loading device into a stable state. Let us assume a specific free energy of $k \rightarrow l$ intervariant transition equal to $\varphi(kl) = \sigma_{ij}[\varepsilon_{ij}(k) - \varepsilon_{ij}(l)]$ and select a volume fraction of favourable martensite variant $\omega \in [0,1]$ as a variable, which de-

TABLE 2. The modes of intervariant transitions in the $10M$, $14M$ and NM martensites of Ni_2MnGa.

Martensite	$10M$	$14M$			$NM(L1_0)$
Mode	*ac*	*ab*	*bc*	*ac*	*ca*
Strain	0.063	0.062	0.046	0.108	0.183

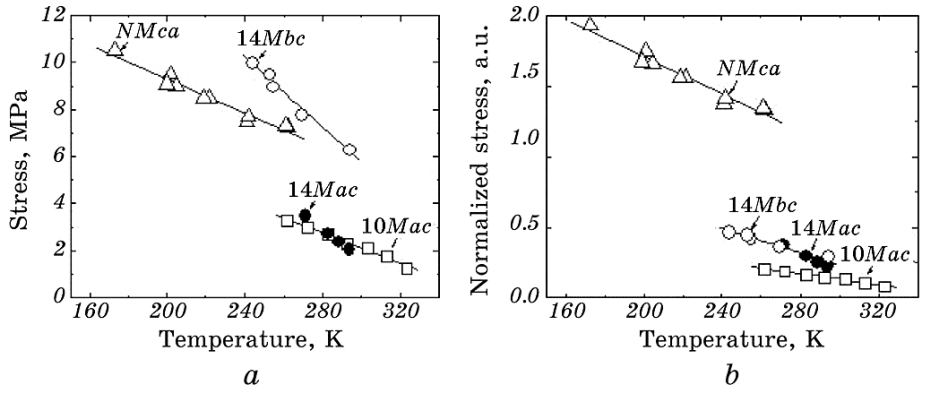

Fig. 4. Stresses of variants' rearrangement in the 10*M*, 14*M* and *NM* martensites.

scribes a state of thermodynamic system. Then, $\sigma_{\text{eff}} = -\partial\varphi(kl)/\partial\omega$ is an effective stress moving a twin boundary at intervariant transition. As we used the only one crystal during the whole research, this stress can be a measure of lattice resistance for the movement of twin boundary in different martensites. Using data of Fig. 4, *a*, the average value of effective stress can be determined at simplifying assumption $\sigma_{\text{eff}}\Delta\omega = \bar{\sigma}_{ij}[\varepsilon_{ij}(k) - \varepsilon_{ij}(l)]$, where $\Delta\omega = 1$ and $\bar{\sigma}_{ij}$ equals to above determined stress of variant rearrangement.

The effective stresses of intervariant transitions in the 10*M*, 14*M* and *NM* martensites are shown in Fig. 4, *b*. First of all, the effective stresses of the intervariant 14*Mbc* and 14*Mac* transitions become equal (within data scattering). As to distinction of effective stresses for the different martensites, there is a certain dependence of these stresses on crystalline structure of martensites. The effective stress of twin boundary motion in perfect tetragonal *NM* martensite is the highest and decreases in the nanotwinned 14*M* and 10*M* martensites with a decrease of period of a nanotwinned structure.

4. CONCLUSIONS

Various modes of stress-induced intervariant transitions in the 10*M*, 14*M*, and $L1_0$ martensites were experimentally realized and discussed on the basis of matrix approach.

Mechanical testing of the same single crystal in different structural states gave an opportunity to compare twinning stresses in the 10*M*, 14*M*, and $L1_0$ martensites of Ni_2MnGa.

The stress of twin boundary motion in perfect $L1_0$ martensite is highest and decreases in the 14*M* and 10*M* martensites with a decrease of period of a nanotwinned structure.

REFERENCES

1. S. J. Murray, M. Marioni, S. M. Allen, and R. C. O'Handley, *Appl. Phys. Lett.*, **77**, No. 6: 886 (2000).
2. A. Sozinov, A. A. Likhachev, N. Lanska, and K. Ullakko, *Appl. Phys. Lett.*, **80**, No. 10: 1746 (2002).
3. A. Sozinov, A. A. Likhachev, N. Lanska, O. Soderberg, K. Ullakko, and V. K. Lindroos, *Mater. Sci. Eng. A*, **378**, Nos. 1–2: 399 (2004).
4. A. Sozinov, N. Lanska, A. Soroka, and W. Zou, *Appl. Phys, Lett.*, **102**: 021902 (2013).
5. P. J. Webster, K. R. A. Ziebeck, S. L. Town, and M. S. Peak, *Philos. Mag. B*, **49**, No. 3: 295 (1984).
6. V. V. Martynov and V. V. Kokorin, *J. Phys. III France*, **2**, No. 5: 739 (1992).
7. K. Otsuka, T. Ohba, M. Tokonami, and C.M. Wayman, *Scr. Met.*, **29**, No. 10: 1359 (1993).
8. V. V. Martynov, *J. Phys. IV France*, **5**, No. C8: 91 (1995).
9. S. Morito and K. Otsuka, *Mater. Sci. Eng. A*, **208**, No. 1: 47 (1996).
10. J. Pons, V. A. Chernenko, R. Santamarta, and E. Cesari, *Acta Mat.*, **48**, No. 12: 3027 (2000).
11. V. Soolshenko, N. Lanska, and K. Ullakko, *J. Phys. IV France*, **112**: 947 (2003).
12. C. Segui, V. A. Chernenko, J. Pons, and E. Cesari, *J. Magn. Magn. Mater.*, **290–291**: 811 (2005).
13. J. Pons, R. Santamarta, V. A. Chernenko, and E. Cesari, *J. Appl. Phys.*, **97**: 083516 (2005).
14. J. Pons, R. Santamarta, V. A. Chernenko, and E. Cesari, *Mater. Sci. Eng. A*, **438–440**: 931 (2006).
15. A. A. Likhachev and K. Ullakko, *EPJ direct*, **1**, No. 1: 1 (2000).
16. A. G. Khachaturyan, S. M. Shapiro, and S. Semenovskaya, *Phys. Rev. B*, **43**, 10832 (1991).
17. M. Zeleny, L. Straka, and A. Sozinov, *MATEC Web of Conferences*, **33**: 05006 (2015).
18. M. Zeleny, L. Straka, A. Sozinov, and O. Heczko, *Phys. Rev. B*, **94**: 224108 (2016).